Fabrication of Multi-Blade Crystals for Hard-X-ray Multi-Beam Imaging System

doi: 10.35848/1347-4065/abaac5

Fabrication of Multi-Blade Crystals for Hard-X-ray Multi-Beam Imaging System

Wataru Yashiro[1]*, Xiaoyu Liang[1], Wolfgang Voegeli[2], Takeshi Wada[3], Hidemi Kato[3], and Kentaro Kajiwara[4]

[1]*Institute of Multidisciplinary Research for Advanced Materials (IMRAM), Tohoku University, Sendai, Miyagi 980-8577, Japan*

[2]*Faculty of Education, Tokyo Gakugei University, Koganei, Tokyo 184-8501, Japan*

[3]*Institute for Materials Research (IMR), Tohoku University, Sendai, Miyagi 980-8577, Japan*

[4]*Japan Synchrotron Radiation Research Institute (JASRI), Sayo, Hyogo 679-5198, Japan*

We report on the fabrication of multi-blade crystals for a hard-X-ray multi-beam imaging system by using silicon microfabrication techniques. Such a crystal consists of several single-crystalline blades, which make different angles to an incident white X-ray beam and reflect X-rays satisfying the Bragg condition in the imaging system. We fabricated two types of multi-blade crystals, one- and two-point-supported, in which blades are connected by one and two bridges to the surrounding part, respectively. The reflected beams from the blades of the two-point-supported crystal were largely distorted, while those of the one-point-supported crystal provided distortion-free reflected beams. We show that multi-angle absorption-contrast X-ray imaging can be achieved using the one-point-supported crystal with sufficient crossing precision.

1. Introduction

X-ray imaging has been widely used for visualizing internal structures in samples that are not transparent to visible light. A projection image of a sample can be obtained even with a temporal resolution on the order of or higher than μs if synchrotron radiation (SR) or X-ray free-electron laser (XFEL) is used,[1–11] but its inner structures in the depth direction cannot be differentiated. X-ray tomography, however, enables us to visualize three-dimensional structures in a sample even with a measurement time of a few ms,[4,5,7,11] but the sample or both the X-ray source and detector has to be rotated to obtain a tens to hundreds of projection images, which are typically required for a tomographic reconstruction.

Several X-ray multi-beam techniques, which can differentiate internal structures in the depth direction, have recently been proposed not only for SR and XFEL facilities[12–16] but also for laboratories.[17–20] In this paper, we report on the fabrication of the multi-blade crystal

*E-mail: wyashiro@tohoku.ac.jp

that can be used for an X-ray multi-beam imaging system for a white SR beam. In the next section, we show the fabrication process for a multi-blade crystal using microfabrication techniques. In Section 3, we present the experimental results from evaluating the two types of multi-blade crystals, one- and two-point-supported, we fabricated with the above process. We show that the reflected beams from the blades of the two-point-supported crystal were largely distorted, while the one-point-support crystal can provide distortion-free projection images for X-ray absorption-contrast imaging with sufficient crossing precision of the reflected X-ray beams. In Section 4, we discuss the causes of the large distortion of the reflected X-ray beams from the two-point-supported crystal and the compatibility of typical X-ray phase-contrast imaging techniques with the X-ray multi-beam imaging system.

2. Fabrication of multi-blade crystal

A schematic of an X-ray multi-beam imaging system is shown in Fig. 1 (a), in which an array of single-crystalline blades with different angles reflect a white SR beam to divide into multiple beams with different energies that satisfy the Bragg condition. Such an X-ray multi-beam imaging system can be constructed by fabricating a thin multi-blade crystal with an array of blades, as shown in Figs 1 (b) and (c), and bending the part surrounding the blades along a curved holder. We fabricated such bendable multi-blade crystals through microfabrication techniques.

Our two types of multi-blade crystals were fabricated in the process shown in Fig. 2. They were fabricated from double-side-polished Si (001) wafers with a thickness of 200 μm. A photoresist pattern with 200 μm-wide lines, which define the outlines of the multi-blade crystals, was first formed on the Si wafer (Figs. 2 (a) and (b)). The Si wafer was spin-coated by OFPR 800 photoresist, which was exposed to ultraviolet (UV) light and developed in tetramethyl ammonium hydroxide (TMAH) solution. The Si wafer was then pasted on a thick substrate (a 500 μm-thick Si wafer) (Fig. 2 (c)), and grooves with a depth of 80 μm were formed on the surface of Si wafer by using a deep reactive ion etching (RIE) system (MUC-21, Sumitomo Precision Products), where SF_6 and C_4H_8 were alternately used (Fig. 2 (d)). Finally, the Si wafer was separated from the substrate with a heated mixture of concentrated H_2SO_4 and H_2O_2 solution (Fig. 2 (e)), and its back side was uniformly wet-etched using KOH solution or dry-etched using inductively-coupled plasma (ICP) to form the desired multi-blade crystals with a thickness of 80 μm (Fig. 2 (f)).

The blades of our one- and two-point supported-type crystals were connected by one and two bridges with widths of 200 μm (see Figs. 1 (b) and (c)), respectively, to the surrounding

part. Figures 3 (a) and 4 (a) show photos of the two- and one-point-supported multi-blade crystals, respectively.

3. Evaluation of multi-blade crystals

We conducted X-ray imaging experiments to evaluate our multi-blade crystals. The experiment was conducted at BL28B2 in SPring-8, Japan, where a white SR beam from a bending magnet is available. Each of the multi-blade crystal was fixed to a cylindrical aluminium holder, as shown in Figs. 3 (b) and 4 (b). Two cylindrical-shape fixtures made of Teflon were used to hold and bend the multi-blade crystal along the curved surface of the holder. The holder with the multi-blade crystal fixed to it was located on the translation and rotation stages (see upper left figure of Fig. 5), by which the position and angle of the crystal relative to the white SR beam were adjusted. Each blade of the multi-blade crystal reflected X-rays with energies that satisfy the Bragg condition when it is illuminated with the white SR beam. The X-ray multi-beam imaging system was designed to focus the X-ray beams reflected from (110) crystal planes, which are perpendicular to the surface of the multi-blade crystal (in the Laue case), to obtain projection images of a sample located at the centre of the focused X-ray beams. We captured the reflected X-ray beams by using an X-ray imaging detector with an effective pixel size of 5 μm, consisting of a 10-μm scintillator screen (Gd_2O_2S : Tb), mirror, relay lenses, and a CMOS camera (Hamamatsu Photonics Corporation, Scientific CMOS Camera: Orca-Flash 2.8). The detector was located 500 mm downstream from the sample.

We first evaluated the quality of the reflected X-rays from the blades of the two-point-supported crystal shown in Fig. 3 (a). The part surrounding the blades was bent along a cylinder with a radius of 645 mm, covering ±1 degrees of the incident angle (±2 degrees of the scattering angle), as shown in Fig. 3 (b). Figure 3 (c) shows an image of a reflected X-ray beam from a blade. In spite of the small curvature of the cylindrical holder, the reflected X-ray beam was largely distorted.

Next, we evaluated reflected X-ray beams from the one-point-supported crystal shown in Fig. 4 (a). Figure 4 (c) shows an image of a reflected X-ray beam from a blade of this crystal. We used a 50-mm radius cylindrical holder (Fig. 4 (b)), which can cover 25 degrees of projection angle. In spite of the large curvature of the cylinder, all the reflected X-ray beams from the one-point-supported crystal was not distorted, even close to the bridge supporting the blade.

Since it was shown that the X-ray beam from the one-point-supported crystal is distortion-free, we demonstrated multi-beam X-ray absorption-contrast imaging using it. We used a

500-μm-diameter Au wire as a sample. The lower figures of Fig. 5 shows transmittance images of the sample for seven scattering angles to the incident X-rays (seven projection angles to the sample, 12.2°, 15.6°, 19.6°, 23.8°, 28.2°, 32.7°, and 37.1°, corresponding to 30.4, 23.8, 19.0, 15.7, 13.2, 11.5, and 10.1 keV for the fundamental (2 2 0) Bragg reflection, respectively). Images of reflected X-ray beams with and without the sample were captured with an exposure time of 5 s (50 ms × 100). From the transmittance images we estimated the crossing precision of the reflected X-ray beams to be ±0.3 mm. Thus, multi-angle absorption-contrast X-ray imaging covering 25 degrees of projection angle was successfully achieved by using the one-point-supported crystal with sufficient crossing precision.

4. Discussion

The reflected beams from the blades of the two-point-supported crystal had large distortion, which might be explained by the torsion of the blades. For example, if the upper bridge of a blade shifts along the curved surface of the 645-mm-radius holder by 0.1 mm relative to the lower bridge, the direction of the reflected X-ray beam from the upper part of the blade may be 0.3 mrad different from that from the lower part as the crystal planes reflecting X-rays is twisted. This difference in direction can cause detectable distortion of the reflected X-ray beam. A shift of the upper bridge in the direction perpendicular to the curved surface can also cause small distortion of the reflected X-ray beam because of the shift in the exit point of the reflected X-rays although the orientation of the (110) crystal planes does not change. Note that the distortion of the reflected X-ray beam shown in Fig. 3 (c) cannot be explained only by the directional change in the crystal planes and the positional change in the surface of the blade because the width of the reflected X-ray beam is not constant but larger near the upper bridge. This spherical-wave effect may be explained by the dynamical focusing or defocusing effect of a slightly bent single-crystalline blade.[21)]

Reflected X-ray beams from blades with different incident angles have different energies, and a reflected X-ray beam from a blade contains even higher harmonics, as shown in a previous paper.[15)] This fact generally makes it difficult to quantitatively interpret the contrast of absorption-contrast images, and assumptions such as homogeneous composition are necessary. Installing a grating-based X-ray interferometer[4,5,7,22–34)] for a reflected beam makes quantitative X-ray phase-contrast imaging possible because it works as an energy filter. In fact, we confirmed that quantitative high-sensitive X-ray phase-contrast imaging is possible with a sufficiently high visibility of moiré fringes by using a reflected X-ray beam from a blade. Propagation-based X-ray imaging,[35–37)] which is another high-sensitive X-ray phase-contrast

imaging technique, was also possible by using the reflected X-ray beam although pseudo-homogeneous assumption[11,38–44] and spectral measurement may be required for quantitative X-ray phase-contrast imaging. Other X-ray phase-contrast imaging techniques such as X-ray crystal interferometry[45–49] and diffraction-enhanced imaging[50–52] should require complex optical systems with high precision to be combined with X-ray multi-beam imaging systems. Thus, the grating-based and propagation-based techniques are the two candidates that are compatible with the X-ray multi-beam imaging system presented in this paper and will allow for much more versatile use of it.

5. Summary

We reported on the fabrication of multi-blade crystals for a hard-X-ray multi-beam imaging system (Fig. 1 (a)) by a microfabrication process (Fig. 2). We fabricated two types of multi-blade crystals (Figs. 1 (b) and (c)), one- and two-point-supported, in which blades are connected by one and two bridges to the surrounding part. It was shown that the reflected beams from the blades of the two-point-supported crystal were largely distorted (Fig. 3 (c)), while those of the one-point-supported crystal provided distortion-free reflected beams (Fig. 4 (c)). We demonstrated multi-beam absorption-contrast X-ray imaging for a Au wire by using the one-point-supported crystal with sufficient crossing precision.

Acknowledgments

The experiment was conducted in SPring-8, Japan. We would like to express our gratitude to Prof. Etsuo Arakawa, Tokyo Gakugei University for fruitful discussion. This research was supported by JST CREST Grant Number JPMJCR1765.

Fig. 1. (a) Schematic of X-ray multi-beam optics consisting of array of single-crystalline blades for X-ray multi-beam imaging. (b)-(c) Designs of our fabricated multi-blade crystals consisting of several single-crystalline blades, which take different angles to incident angle when surrounding part is bent ((b) two-points-supported and (c) one-point-supported crystals).

Fig. 2. Fabrication process of multi-blade crystal through microfabrication techniques.

Fig. 3. (a,b) Photos of fabricated two-point-supported multi-blade crystal (a) and 645-mm-radius cylindrical holder with multi-blade crystal fixed to it (b). (c) Reflected X-ray beam from upper part of blade of this crystal (Scale bar: 500 μm).

Fig. 4. (a,b) Photos of fabricated one-point-supported multi-blade crystal (a) and 50-mm-radius cylindrical holder with multi-blade crystal fixed to it (b). (c) Reflected X-ray beam from blade of this crystal (Scale bar: 500 μm).

Fig. 5. Upper: photos of sample (500-μm-diameter Au wire) and 50-mm radius cylindrical holder with multi-blade crystal. Lower: transmittance (absorption-contrast) images of sample for different scattering angles (projection angles) (scale bar: 500 μm; gray scale: 0-1.2)

References

1) J.J. Socha, M.W. Westneat, J.F. Harrison, J.S. Waters, and W.K. Lee, BMC Biol. **5**, 6 (2007)
2) J.S. Lee, B.M. Weon, S.J. Park, J.H. Je, K. Fezzaa, and W.K. Lee, Nature Commun. **2**, 367 (2011).
3) A. Rack, M. Scheel, L. Hardy, C. Curfs, A. Bonnin, H. Reichert, J. Synchrotron Rad. **21**, 815 (2014).
4) W. Yashiro, D. Noda, and K. Kajiwara, Appl. Phys. Express **10**, 052501 (2017).
5) W. Yashiro, R. Ueda, K. Kajiwara, D. Noda, and H. Kudo, Jpn. J. Appl. Phys. **56**, 112503 (2017).
6) M. P. Olbinado, X. Just, J.-L. Gelet, P. Lhuissier, M. Scheel, P. Vagovic, T. Sato, R. Graceffa, J. Schulz, A. Mancuso, J. Morse, and A. Rack, Opt. Express **25**, 13857 (2017).
7) W. Yashiro, C. Kamezawa, D. Noda, and K. Kajiwara, Appl. Phys. Express **11**, 122501 (2018).
8) M. P. Olbinado, J. Grenzer, P. Pradel, T. De Resseguier, P. Vagovic, M.-C. Zdora, V.A. Guzenko, C. David, and A. Rack, J. Instrum. **13**, C04004 (2018).
9) E. M. Escauriza, M. P. Olbinado, M. E. Rutherford, D. J. Chapman, J. C. Z. Jonsson, A. Rack, and D. E. Eakins, Appl. Opt. **57**, 5004 (2018).
10) P. Vagovič, T. Sato, L. Mikeš, G. Mills, R. Graceffa, F. Mattsson, P. Villaueva-Perez, A. Ershov, T. Faragó, J. Uličný, H. Kirkwood, R. Letrun, R. Mokso, M.-C. Zdora, M. P. Olbinado, A. Rack, T. Baumbach, J. Schulz, A. Meents, H. N. Chapman, and A. P. Mancuso, Optica **6**, 1106 (2019).
11) F. García-Moreno, P.H. Kamm, T.R. Neu, F. Bülk, R. Mokso, C. M. Schlepütz, M. Stampanoni, and J. Banhart, Nat Commun. **10**, 3762 (2019).
12) M. Hoshino, T. Sera, K. Uesugi and N. Yagi, JINST **8**, C05002 (2013).
13) P. Villanueva-Perez, B. Pedrini, R. Mokso, P. Vagovič, V. A. Guzenko, S. J. Leake, P. R. Willmott, P. Oberta, C. David, H. N. Chapman, and M. Stampanoni, Optica **5**, 1521 (2018).
14) W. Yashiro, T. Shirasawa, C. Kamezawa, W. Voegeli, E. Arakawa, and K. Kajiwara, Jpn. J. Appl. Phys. **59**, (2020) 038003.
15) W. Voegeli, K. Kajiwara, H. Kudo, T. Shirasawa, X. Liang, and W. Yashiro, Optica **7**, (2020) 514-517
16) T. Shirasawa, X. Liang, W. Voegeli, E. Arakawa, K. Kajiwara, and W. Yashiro, Appl.

Phys. Express (2020), in press.

17) M. Bieberle, F. Barthel, H.-J. Menz, H.-G. Mayer, and U. Hampel, Appl. Phys. Lett. **98**, 034101 (2011).

18) G. Yang, X.Qian, T.Phan, F.Sprenger, S.Sultana, X.Calderon-Colon, B.Kearse, D. Spronk, J.Lu, O.Zhou, Nucl. Instrum. Methods Phys. Res. A **648**, S220 (2011).

19) K. M. Sowa, B. R. Jany, and P. Korecki, Optica **5**, 577 (2018).

20) A. Cramer, J. Hecla, D. Wu, X. Lai, T. Boers, K. Yang, T. Moulton, S. Kenyon, Z. Arzoumanian, W. Krull, K. Gendreau and R. Gupta, Sci. Rep. **8**, 14195 (2018).

21) J.-P. Guigay, C. Ferrero, D. Bhattacharyya, O. Mathon, and S. Pascarelli, Acta Cryst. **A69**, 91 (2013).

22) C. David, B. Nöhammer, and H. H. Solak, Appl. Phys. Lett. **81**, 3287 (2002).

23) A. Momose, S. Kawamoto, I. Koyama, Y. Hamaishi, K. Takai, and Y. Suzuki, Jpn. J. Appl. Phys. **42**, L866 (2003).

24) T. Weitkamp, A. Diaz, C. David, F. Pfeiffer, M. Stampanoni, P. Cloetens, and E. Ziegler, Opt. Express **13**, 6296 (2005).

25) A. Momose, W. Yashiro, and Y. Takeda, Jpn. J. Appl. Phys. **45**, 5254 (2006).

26) F. Pfeiffer, T. Weitkamp, O. Bunk, and C. David, Nat. Phys. **2**, 258 (2006).

27) W. Yashiro, Y. Takeda, and A. Momose, J. Opt. Soc. Am. A **25**, 2025 (2008).

28) F. Pfeiffer, T. Weitkamp, O. Bunk, and C. David, Nat Mater. **7**, 134 (2008).

29) W. Yashiro, Y. Terui, K. Kawabata, and A. Momose, Opt. Express **18**, 16890 (2010).

30) W. Yashiro and A. Momose, Opt. Express **23**, 9233 (2015).

31) W. Yashiro, P. Vagovič, and A. Momose, Opt. Express **23**, 23462 (2015).

32) W. Yashiro, D. Noda, and K. Kajiwara, Opt. Express **26**, 1012 (2018).

33) W. Yashiro, Microscopy **67**, 303 (2018).

34) W. Yashiro, S. Ikeda, Y. Wada, K. Totsu, Y. Suzuki, and A. Takeuchi, Sci. Rep. **9**, 14120 (2019).

35) A. Snigirev, I. Snigireva, V. Kohn, S. Kuznetsov, and I. Schelokov, Rev. Sci. Instrum. **66**, 5486 (1995).

36) S.W. Wilkins, T.E. Gureyev, D. Gao, A. Pogany, A.W. Stevenson, Nature **384**, 335 (1996).

37) P. Cloetens, R. Barrett, J. Baruchel, J.-P Guigay, and M. Schlenker, J. Phys. D **29**, 133 (1996).

38) D. Paganin, S. C. Mayo, T. E. Gureyev, P. R. Miller, and S. W. Wilkins, J. Microsc. **206**, 33 (2002).

39) A. V. Bronnikov, J. Opt. Soc. Am. A **19**, 472(2002).

40) R. C. Chen, L. Rigon, and R. Longo, Opt. Express, **21**, 7384 (2013).

41) A. Groso, R. Abela, and M. Stampanoni, Opt. Express, **14**, 8103 (2006).

42) S. M. Walker, D. A. Schwyn, R. Mokso, M. Wicklein, T. Müller, M. Doube, M. Stampanoni, H. G. Krapp, and G. K. Taylor, PLoS Biol. **12**, e1001823 (2014).

43) L. Xu, R. C. Chen, G. H. Du, Y. M. Yang, F. X. Wang, B. A. Deng, H. L. Xie, and T. Q. Xiao, Sci. Rep. **6**, 32380 (2016).

44) A. Ruhlandt, M. Töpperwien, M. Krenkel, R. Mokso, and T. Salditt, Sci. Rep. **7**, 6487 (2017).

45) U. Bonse and M. Hart, Appl. Phys. Lett. **7**, 99 (1965).

46) A. Momose and J. Fukuda, Med. Phys. **22**, 375 (1995).

47) A. Yoneyama, N. Amino, M. Mori, M. Kudoh, T. Takeda, K. Hyodo, and Y. Hirai, Jpn. J. Appl. Phys. **45**, 1864–1868 (2006).

48) T. Takeda, A. Yoneyama, J. Wu, T.-T. Lwin, A. Momose, and K. Hyodo, J. Synchrotron Rad. **19**, 252-256 (2012).

49) A. Yoneyama, A. Iizuka, T. Fujii, K. Hyodo, and J. Hayakawa, Sci. Rep. 8:12674 (2018).

50) J. Davis, D. Gao, T. E. Gureyev, A. W. Stevenson, and S. W. Wilkins, Nature **373**, 595 (1995).

51) D. Chapman, W. Thomlinson, R. E. Johnston, D. Washburn, E. Pisano, N. Gmür, Z. Zhong, R. Menk, F. Arfelli, and D. Sayers, Phys. Med. Biol. **42**, 2015 (1997).

52) M. Ando, H. Sugiyama, A. Maksimenko, W. Pattanasiriwisawa, K. Hyodo, and Z. Xiaowei, Jpn. J. Appl. Phys. **40**, L844 (2001).

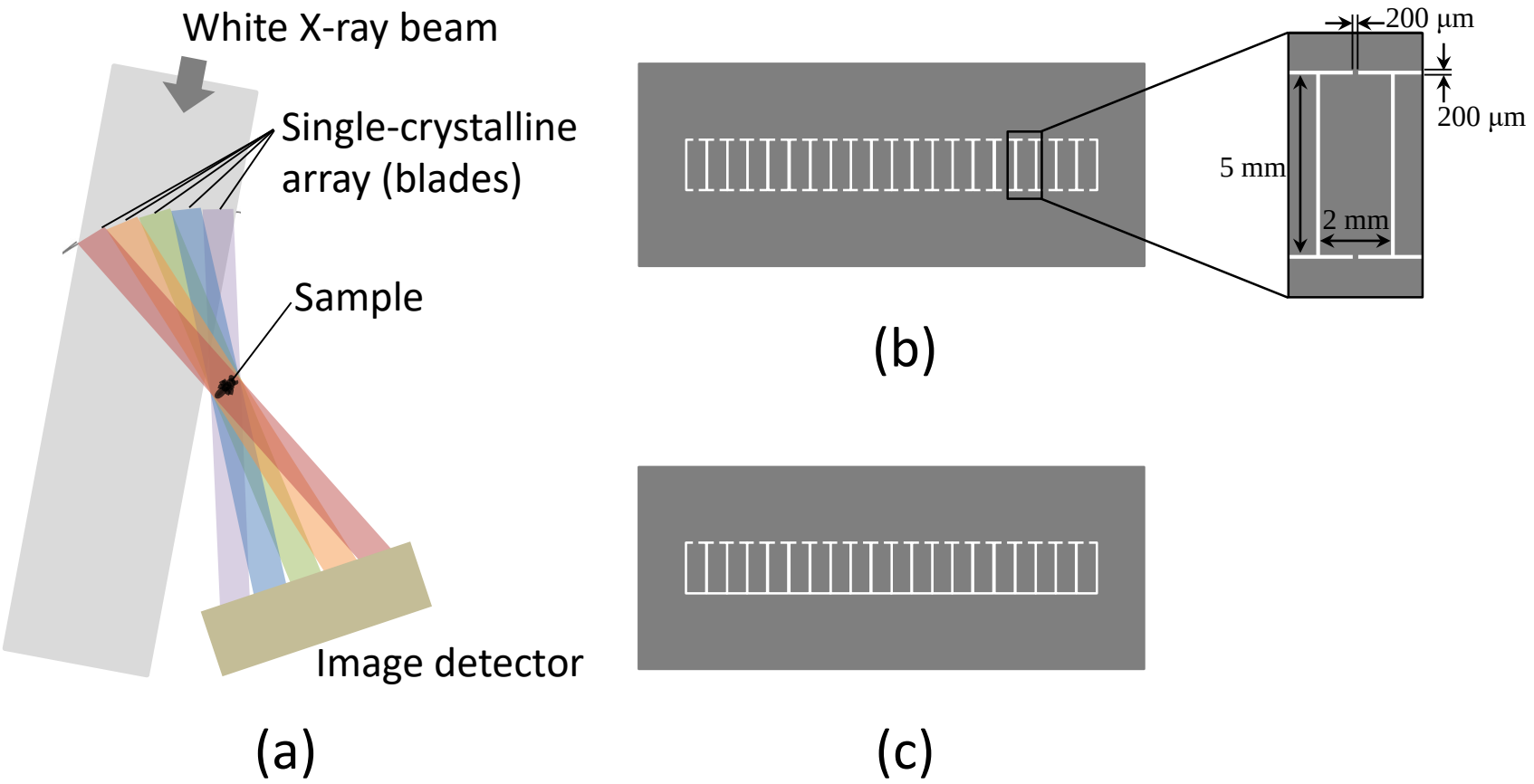

Fig. 1 W. Yashiro et al.

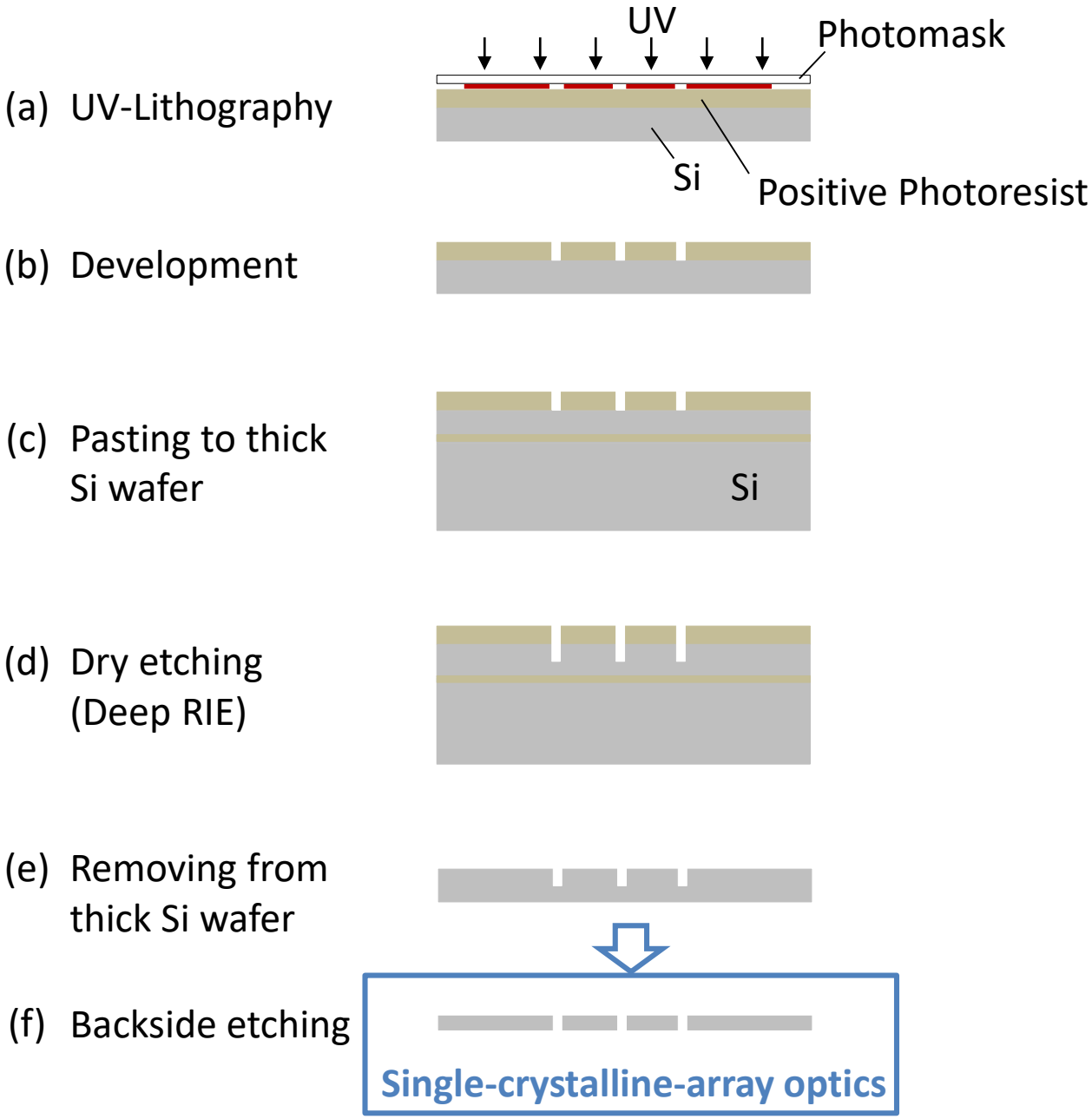

Fig. 2 W. Yashiro et al.

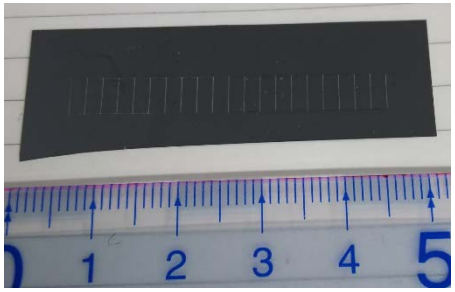

(a)

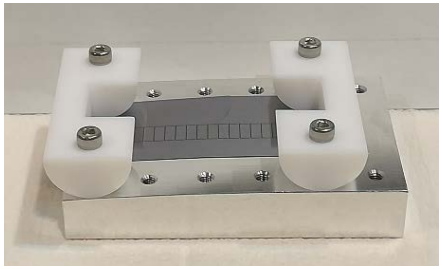

(b)

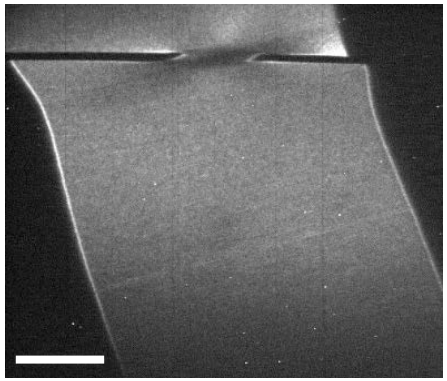

(c)

Fig. 3 W. Yashiro et al.

(a)

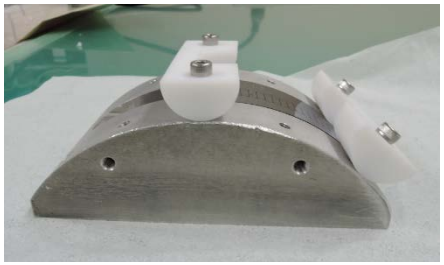

(b)

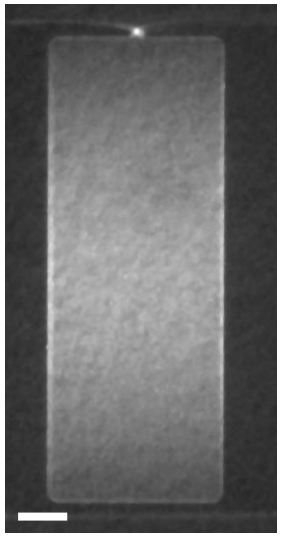

(c)

Fig. 4 W. Yashiro et al.

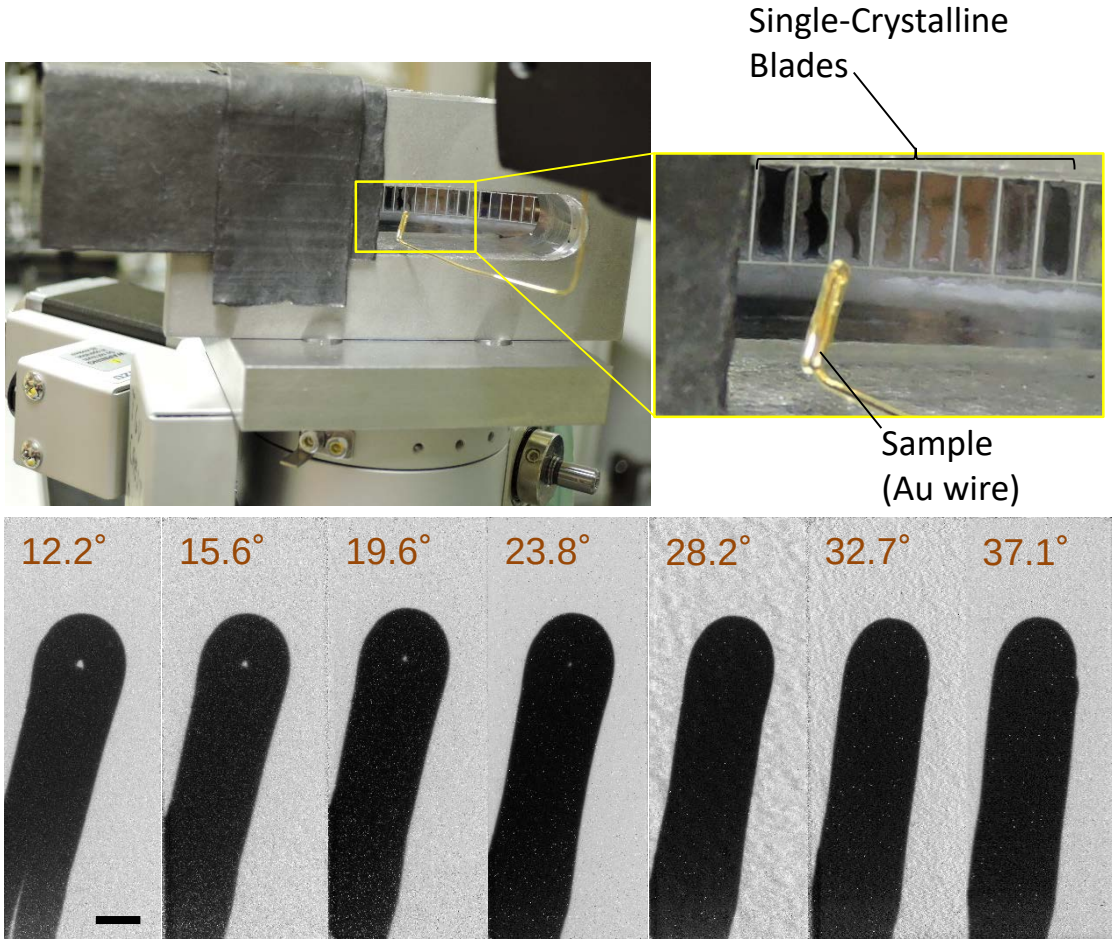

Fig. 5 W. Yashiro et al.